JOURNAL OF GEOPHYSICAL RESEARCH, VOL. 92, NO. C7, PAGES 7017–7031, JUNE 30, 1987

Dynamics and Thermodynamics of the Ice/Upper Ocean System in the Marginal Ice Zone of the Greenland Sea

MILES G. MCPHEE

McPhee Research Company, Yakima, Washington

GARY A. MAYKUT

Department of Atmospheric Sciences, University of Washington, Seattle

JAMES H. MORISON

Polar Science Center, University of Washington, Seattle

Measurements were made of the ice/upper ocean system in the marginal ice zone of the Greenland Sea during a 4-day storm in which wind blew the ice south across a frontal region, coinciding with the ice edge that had existed when the storm began. In response to wind stress of about 0.2 Pa, a turbulent boundary layer developed under the ice that exhibited marked Ekman rotation in both mean velocity (average surface speed about 0.17 m s^{-1}, deflection angle about 33°) and turbulent stress profiles (typical Reynolds stress about 0.1 Pa). Ablation of the ice undersurface increased rapidly after crossing the surface temperature front, and the observed melt rate corresponded with direct heat flux measurements in the oceanic boundary layer, with maximum upward heat flux of about 200 W m^{-2}. We discuss overall momentum and energy balances, interpret observed boundary layer measurements with a numerical model, and show that molecular effects are important for heat and mass transport at the hydraulically rough ice-ocean interface. We also develop a simple model for predicting ice melt from interfacial stress and temperature and salinity of the mixed layer.

1. INTRODUCTION

In the open ocean, fluxes of energy, mass, and momentum at the air-sea interface govern the structure and extent of the oceanic mixed layer, which is primarily responsible for moderating seasonal variation in surface temperature on a global scale. The efficiency with which wind stress can mix the upper ocean is strongly influenced by density gradients near the surface; thus the depth and temperature of the mixed layer depend in an intricate way upon the wind stress, radiation balance, evaporation/precipitation balance, and turbulent heat exchange with the atmosphere. At high latitudes, sea ice plays a pivotal role in air-sea interaction, by reflecting much of the incoming solar radiation and by insulating the ocean from direct sensible and latent heat exchange with the atmosphere. Ice also influences the mechanical mixing imparted by wind, in some cases absorbing most of the wind stress and, in others, enhancing wind stress by increasing the surface roughness. Storage of heat in an ice-covered ocean is dominated by latent exchanges as ice grows and decays; thus seasonal mixed-layer temperature variability is small. But since sea ice excludes most of the salt as it freezes, mixed-layer density undergoes a seasonal cycle analogous to that of temperate oceans, except that density is controlled almost exclusively by salinity [*Morison and Smith*, 1981].

In the marginal ice zone (MIZ), the open and ice-covered regimes meet across a narrow strip that exhibits extreme gradients in albedo, sea surface temperature and salinity, atmospheric boundary layer stability, and wind drag. A primary goal of the Marginal Ice Zone Experiment (MIZEX) is to measure and understand how changes in momentum and energy exchange across the MIZ affect the physical response of the air-ice-sea system, including ice extent [*McPhee*, 1983*a*].

In the open ocean, stress at the navifacial interface is usually equated with turbulent stress in the lower part of the atmospheric boundary layer. When ice is present, this balance no longer holds, so physics of momentum transfer in ice-covered oceans has been studied extensively, beginning with Nansen's observations that the Coriolis effect caused ice on which the *Fram* drifted to veer consistently to the right of the surface wind [*Ekman*, 1905]. *Hunkins* [1966] noted the so-called Ekman spiral in current measurements from Fletcher's Ice Island (T-3). *Smith* [1974] and *McPhee and Smith* [1976] measured turbulent (Reynolds) stress and mean flow velocity across the entire boundary layer under pack ice at the Arctic Ice Dynamics Joint Experiment (AIDJEX) pilot study stations. *Langleben* [1980, 1982] also measured Reynolds stress directly near the interface under first-year and multiyear ice. Interfacial stress has been inferred from mean velocity profiles measured under ice [e.g., *Untersteiner and Badgley*, 1965; *Johannessen*, 1970], while *McPhee* [1979] and *Pease et al.* [1983] used methods based on the ice momentum equation to derive underice roughness. A pattern that emerges from these studies is that local stress and profile measurements (especially those made under smooth areas of multiyear pack ice) indicate smaller roughness than that implied by the large-scale balance of forces acting on the ice pack. This apparently results from form drag on pressure ridge keels and other subsurface fea-

Paper number 7C0065.
0148-0227/87/007C-0065$05.00

tures that are not manifested directly in the local turbulent structure near the interface. Understanding how total drag is partitioned in the underice boundary layer remains unresolved.

Another outstanding problem in ice-ocean interaction is describing heat and mass transfer at the ice-ocean interface and in the turbulent boundary layer. In the MIZ, sea ice often drifts into water that is above freezing and melts rapidly, even at times when ice would otherwise grow [*Pease*, 1980]. *McPhee* [1983*b*] used similarity theory (based on scaling that incorporated both rotational and buoyancy effects) to relate melt rate at the ice undersurface to kinematic interfacial stress (u_*^2), mixed-layer salinity minus ice salinity, and change in temperature across a steady, horizontally homogeneous, planetary boundary layer (PBL). McPhee expressed thermal driving in terms of the change in temperature across the PBL, without specifying temperature at $z = -|z_0|$, the upper boundary of the turbulent PBL. *Josberger* [1983] developed a similar treatment, except that he neglected buoyancy effects and specified temperature at z_0 to be freezing, proportional to salinity at the same level. Josberger's approach allows melt rate to be calculated directly from u_* and far-field temperature and salinity, but *McPhee* [1984] pointed out that Josberger's boundary condition neglected temperature and salinity gradients in a "viscous sublayer" near the interface, which may be important for heat and mass transfer, even if the surface is hydraulically rough. Since typical values of z_0 for sea ice are relatively large (0.01–0.1 m), neglect of the sublayer is difficult to justify. *Ikeda* [1986] used the same freezing-line relationship, applied at z_0, to relate ice ablation to specified far-field temperature in his time-dependent implementation of the Mellor-Yamada "level 2" PBL turbulence model. *Mellor et al* [1987] applied the "level 2.5" Mellor-Yamada model to the time-dependent, horizontally homogeneous boundary layer, but they reasoned that the roughness lengths for heat and salt (essentially integration constants for the nondimensional, logarithmic profiles) would be much smaller than for momentum. This allows significant temperature and salinity differences between the ice surface (where the equilibrium freezing condition holds) and z_0, which decreases predicted melt rates, relative to models in which the freezing condition is applied at z_0.

Observational results from the MIZEX experiments (including data presented below) are beginning to resolve some of the theoretical uncertainties. *Josberger* [this issue] presents measurements of bottom ablation near the ice edge in the Bering and Greenland seas. *Josberger and Meldrum* [1985] showed that the bulk heat transfer coefficient for their measurements in the Bering Sea (8×10^{-4}) was only a fraction of the lowest range of reported drag coefficients (they cite *Langleben* [1980], who found z_0 to be only 1.9 mm). If the logarithmic profile is assumed valid for both momentum and scalar contaminants (heat and salt), their result implies either that the surface is much smoother for heat and salt, as argued by *Mellor et al.* [1986], or that Reynolds' analogy (i.e., that scalar diffusivities are roughly the same as eddy viscosity) is not applicable. In the present paper, we present results that indicate that a quasi-laminar sublayer, which none of the studies cited above considers explicitly, is an important aspect of the problem and suggest a simple method for including it in boundary conditions.

For the 1984 MIZEX experiment, the ice-strengthened research vessel *Polar Queen* was moored to ice floes initially located 50–70 km inside the ice edge, and allowed to drift passively while measurements were made of the ice, atmosphere, and ocean in the vicinity of the ship. Our intent was to monitor changes in the air-sea-ice system as we drifted from an environment typical of the high Arctic into the MIZ. The actual drift occurred in two segments. The *Polar Queen* was initially deployed during a "northerly outbreak," throughout which persistent northwesterly winds drove the ice pack and ship south for about 7 days, until the wind reversed and swell near the ice edge broke up the floe to which we were moored. The ship was then redeployed about 60 km northwest and remained moored to one floe for the remaining 30 days of the drift project, from day 170 to 200.

Combined results from ice and upper ocean studies during the entire *Polar Queen* drift are presented in two papers. The general character of ice and upper ocean exchange and its variation over a wide range of conditions (e.g., complete time series of drag and heat transfer coefficients) are described by *Morison et al.* [this issue]. In this paper we focus on a particular period from 1200 UT on July 6, 1984 (day 188), to early on July 10, (day 192), when a small storm with NW winds drove the ship and surrounding ice about 70 km south across the location of the ice edge that had existed when the wind started. The fastest drift and most intense turbulent mixing occurred during this time. Initially, ice concentration was high, the upper ocean was near its freezing temperature, and ice ablation was slow. As we drifted south, the ice pack diverged, mixed-layer temperatures rose abruptly, and our floe began to melt rapidly. We measured the response of the ice-ocean system to these events in unprecedented detail, using a coordinated cross-disciplinary strategy to interrelate measurements of wind, air temperature and humidity, surface radiation, ice mass balance, oceanic turbulent stress and heat flux, and detailed profiles of upper ocean temperature, salinity, and mean velocity.

The paper is organized as follows. Experimental apparatus is described briefly in section 2. Drift during the storm is described in general terms in section 3, which includes discussion of the overall heat and salt budgets. Section 4 presents more detailed results from the measurement programs, including turbulent stress and mean velocity data from the ice-ocean boundary layer, which have never before been measured in an environment as complex as the MIZ. We also introduce calculations from a numerical model of upper ocean dynamics. Our intent is not so much to simulate observed behavior directly, as to provide a template for comparing measurements made in the MIZ with results expected under idealized, horizontally homogeneous conditions. In section 5 we discuss heat and mass transfer and use what we believe to be the first direct measurements of turbulent heat flux in the ice-ocean boundary layer to develop a simple parameterization of heat and salinity flux. Section 6 is a summary.

2. Experimental Program

Measurements made at the upper surface of the ice floe adjacent to the ship included wind stress and sensible heat flux, incident shortwave and longwave radiation, total and spectral albedos, and ice temperature and local pond coverage. Ice ablation was monitored daily at the top, bottom, and

edges of the floe. Incoming longwave and shortwave radiation were sampled at 10-min intervals throughout the experiment. Ground-based measurements of total and spectral albedo were made periodically over the major surface types. Complementary data included internal ice temperature, lead conditions, melt pond depth and coverage, and downwelling spectral irradiance. Local estimates of ice concentration were made daily from the ship, while regional changes between the ship and the ice edge were calculated using a new photometric method that takes advantage of spectral albedo differences between ice/snow, ponds, and open water. Aerial albedo data taken at 500, 650, and 1000 nm during routine helicopter photoflights from the *Polar Queen* were used to construct a system of linear equations that were then inverted to obtain the relative area occupied by ponds, ice, and leads at frequent intervals along the track. With information on ice concentration and pond coverage, it was possible to calculate spatial changes in solar input to the ocean as well as to the ice.

Ice velocity was determined by fitting geographical position data from satellite navigation equipment on board the moored ship, using a complex demodulation technique described by *McPhee* [1986*a*]. The technique decomposes the velocity over a 24-hour period into a mean component, plus rotating inertial and tidal signals, each with clockwise and counterclockwise elements. By performing the least squares fit every 3 hours, a continuous velocity record was synthesized, and tidal and inertial motions removed from the instantaneous velocity.

In the ocean a vector velocity, temperature, and salinity profiler called the Arctic Profiling System (APS) was used to sample the upper 250 m of the ocean at least once every 3 hours and, often, more frequently. The APS measures temperature, conductivity, and three components of velocity. The relative water velocity is converted to earth-centered coordinates using output from a flux gate slaved, directional gyro (bearing) and two accelerometers (tilts). The original system, described by *Morison* [1978, 1980], was modified for MIZEX to use digital electronics based on the Sea-Bird conductivity, temperature, and depth (CTD) design. The instrument samples 12 times per second as it is lowered through the water column at speeds up to 1 m s^{-1}. During MIZEX the system was lowered from a self-contained boat/sled vehicle, which housed the winch and data collection electronics. The data were averaged over 1 s in the field, and during analysis the CTD data were averaged over 2 m and the velocity data over 20 m.

Mean velocity, temperature, and conductivity, along with turbulent stress and turbulent heat flux, were measured at several fixed levels (1, 2, 4, 7, and 15 m from the ice underside) using clusters of three small current meters arranged along orthogonal axes, mounted near fast response Sea-Bird temperature and conductivity meters.

Smith [1978], *Morison* [1980], and *McPhee* [1986*b*] discuss calibration and mounting of the partially ducted current rotors used in the APS and turbulence cluster instruments. According to *Smith* [1978], the head-on calibration is linear with rotation frequency, with accuracy for individual rotors being the larger of 0.1 cm s^{-1} or $\pm 0.5\%$ of actual reading, while precision for the rotors as a group is the larger of 0.3 cm s^{-1} or $\pm 1.2\%$ actual reading. Correction for angle of attack introduces error of about 2% of actual reading. For MIZEX the clusters were calibrated in their assembled configuration by towing through still water at constant speed [*McPhee*, 1986*b*]. These tests showed variability in calibration of the assembled clusters similar to that reported by *Smith* [1978] and showed that variation associated with changes in angle of attack (pitch and yaw) was comparable to rotor-to-rotor variation. During the experiment, alignment of the clusters was monitored continuously and adjusted if the mean horizontal flow vector departed by more than $\pm 20°$ from the optimal orientation in which the component of mean flow sensed by all three rotors is the same. *Morison* [1980] showed that horizontal velocities measured with the APS are accurate to 1 cm s^{-1} in speed and 7° in direction for speeds under 15 cm s^{-1} and depths less than 100 m. For greater depths and speeds, APS speeds begin to read low by 10–15%, due to motion of the device. The manufacturer's stated accuracies for the Sea-Bird temperature and conductivity sensors used in the APS and turbulence clusters are ± 0.01°C per 6 months and ± 0.001 S m^{-1} per month, respectively. Intercomparison between the APS and clusters indicates these tolerances to be conservative. Temperature and conductivity meters were calibrated before and after the experiment.

Sea ice provides a remarkably steady platform that moves with the maximum velocity of the surface boundary layer, which allows us to make measurements of turbulence in the oceanic PBL [*McPhee*, 1986*b*] that would be exceptionally difficult in other circumstances. Except for short maintenance and orientation adjustment periods, three components of velocity, along with temperature and conductivity, were measured six times per second at six levels beneath the ice during the entire storm. Turbulent velocity measurements were processed by separating the time series into 15-min blocks, calculating the mean vector and covariance matrix for each cluster over each time block, then rotating the mean vector and covariance (Reynolds stress) tensor into an east-north-vertical reference frame in which the mean vertical velocity component vanished. Since the time scale of eddies that contribute most to the turbulent energy is typically 1–5 min, a number of these 15-min samples must be smoothed or block averaged to arrive at stable turbulence statistics. The end product is mean horizontal velocity and the Reynolds stress tensor, which includes the turbulent kinetic energy (sum of the diagonal elements) and the horizontal traction at each level ($\langle u'w' \rangle i + \langle v'w' \rangle j$, where i and j are unit vectors). Similar techniques were used for processing the fast response temperature data to get mean temperature and vertical heat flux, $\langle w'T' \rangle$, at each level.

3. General Description of the Drift

The fitted trajectory of the *Polar Queen* from day 188 (July 6, 1984) to day 193 is shown in Figure 1, along with the ice edge that existed on day 188, drawn from a mosaic of airborne synthetic aperture radar (SAR) images taken in the morning of day 188 (R. A. Shuchman et al., Remote sensing of the Fram Strait marginal ice zone, submitted to *Science*, 1986). The original SAR mosaic shows nebulous bands and filaments of ice southeast of the feature shown as a semicircle centered at about 80°N, 2°E, suggestive of an eddy like those often observed along the Greenland Sea ice edge.

In narrative form, the drift is described as follows. When the wind started blowing late in the morning of day 188, ice velocity rapidly reached a dynamic balance with surface wind stress, as a turbulent PBL developed under the ice. Wind and drift velocities (after removing inertial and tidal signals) were

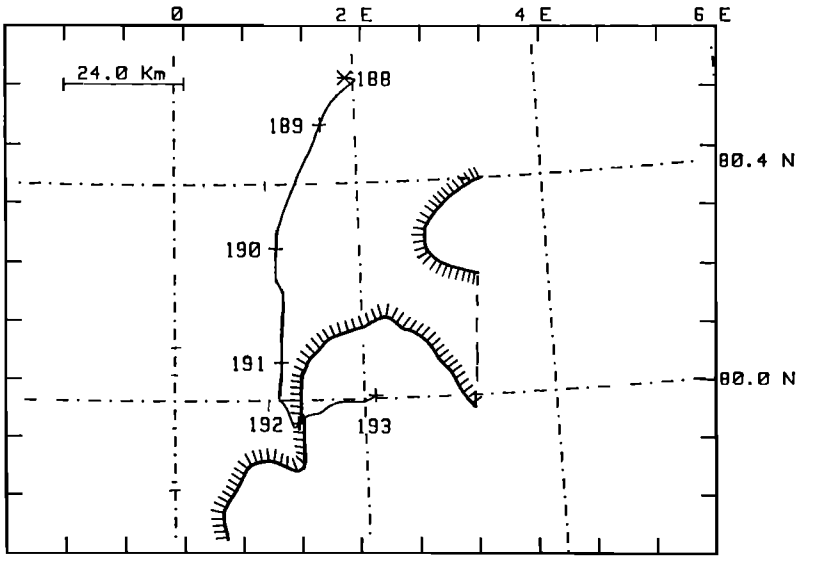

Fig. 1. Trajectory of the *Polar Queen* from day 188 to day 193. Time marks indicate position at 0000 UT on day shown. Also shown is the approximate ice edge as inferred from a mosaic of synthetic aperture radar images taken in the morning of day 188 (R. A. Shuchman et al., Remote sensing of the Fram Strait marginal ice zone, submitted to *Science*, 1986).

for the most part closely correlated (Figures 2*a* and 2*b*), except that on day 190, the wind backed and slackened with no corresponding speed decrease or direction change in ice drift. Temperature, salinity, and density of the upper 150 m of the water column are shown in Figure 3. Turbulent entrainment deepened the mixed layer from less than 10 m to more than 20 m in the first day, and the ice continued to melt slowly. Shortly before 1200 UT on day 190, the floe drifted over a change in upper ocean salinity that forced the base of the mixed layer up to less than 10 m (Figure 3*b*). Eight hours later, it crossed an abrupt temperature front through which the near-surface temperature changed by about 1.5°C (Figure 3*a*). The combined changes had dramatic impact on the dynamics and thermodynamics of the system: ice continued to drift south at

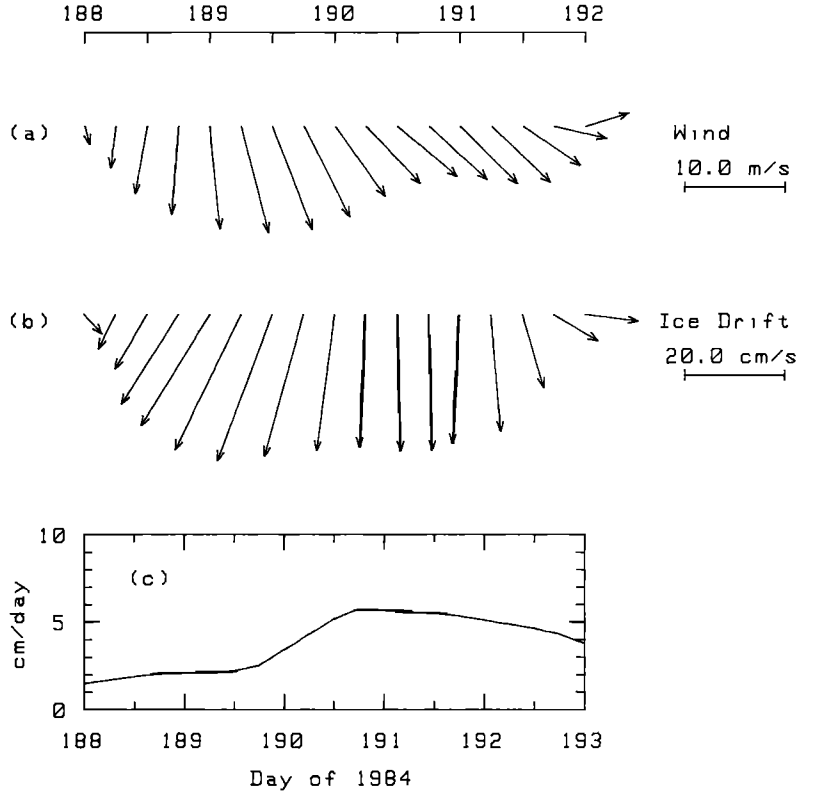

Fig. 2. (*a*) Smoothed wind vectors at 6-hour intervals, as measured over the ice floe, adjusted to the 10-m level. North is up. (*b*) Ice drift velocity, smoothed to eliminate inertial and tidal oscillations, determined by fitting satellite navigation data. (*c*) Combined average surface and bottom melt rate, from daily ablation measurements.

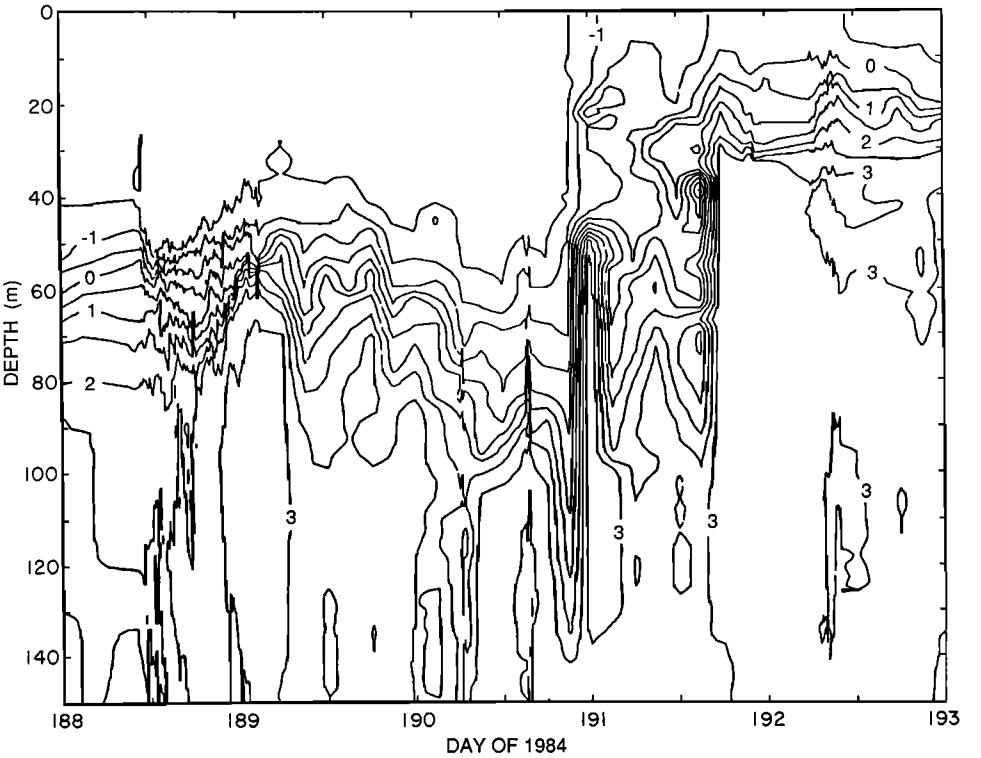

Fig. 3a

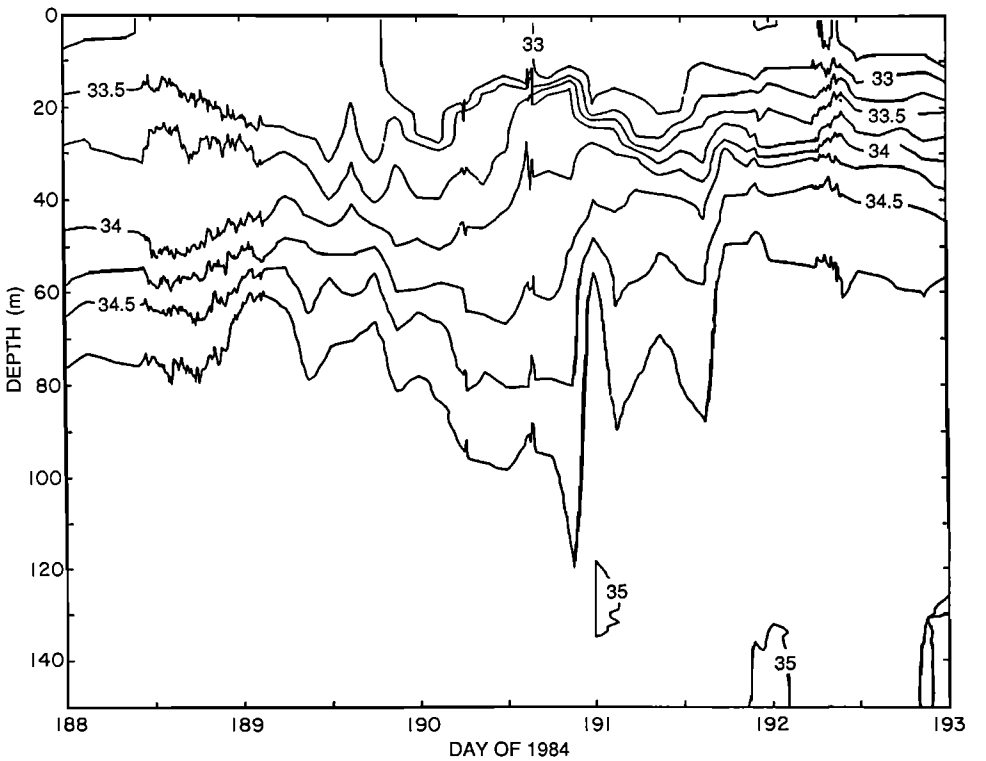

Fig. 3b

Fig. 3. (*a*) Contours of temperature in the upper ocean, days 188–193. Contour interval is 0.5°C. (*b*) Contours of salinity. Contour interval is 0.25 ppt. (*c*) Contours of sigma-*t*. Contour interval is 0.2.

about the same speed, despite decreased wind stress (implying ice divergence); baroclinic jets developed in the stratified fluid just below the mixed layer, and ice ablation increased rapidly (Figure 2*c*). The location of the surface temperature front when we crossed it at about 2100 UT on day 190, was within roughly 3 km of a well-defined ice edge that had existed about midday on 188 (Figure 1). By late on day 191, ice to the east and south of our floe had moved well beyond the initial ice edge. Earlier that day, a photoreconnaissance flight from the ship SE to the ice edge [*Hall*, 1984] showed substantial diver-

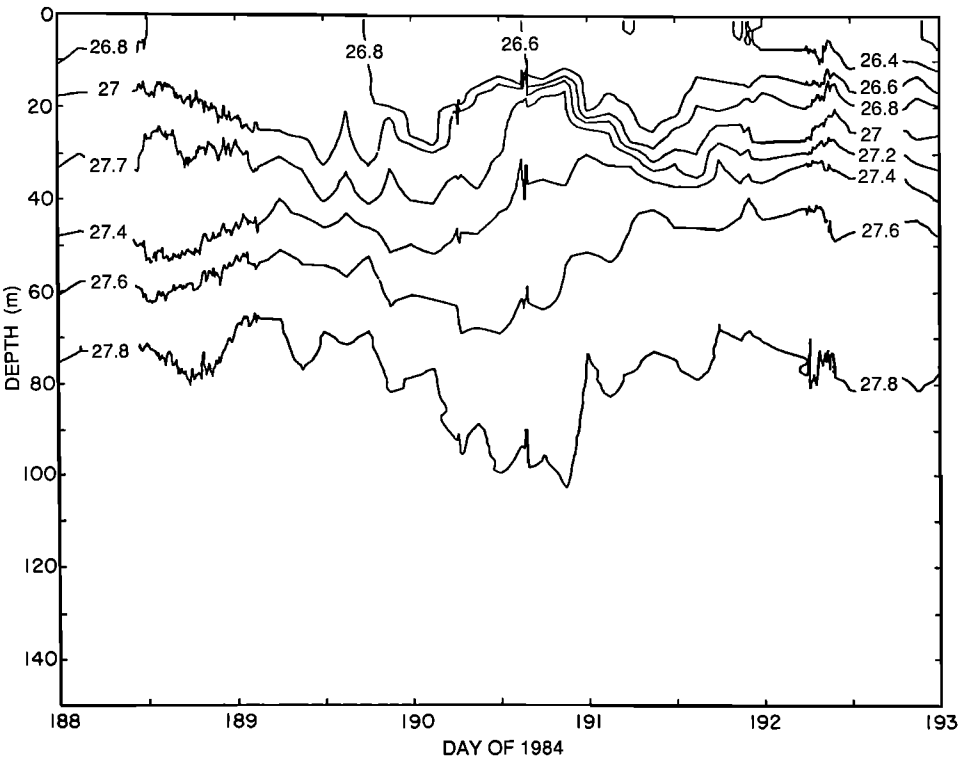

Fig. 3c

gence, with ice concentration remaining high (85%) for the first 10 km, the falling rapidly to 50% or less in the outer 45 km.

During this entire period, the ship appears to have been only a few kilometers east of the pronounced oceanic front that separates cold, relatively fresh water flowing south from the Arctic Ocean along the East Greenland Shelf, from the warmer, saltier water of the Greenland Sea Gyre to the east [*Morison et al.*, this issue]. Buoys initially deployed just west of the ship diverged rapidly to the south, probably in response to surface geostrophic currents associated with the rise in dynamic topography to the west. Evidence of this is found in Figure 3, where the steady decrease in temperature and salinity at, e.g., the 70-m level from 1200 UT on day 189 to 0000 UT on day 190, coincides with westward incursion into the frontal region. The gradual depression of isotherms and isohalines ended abruptly late on day 190, as the ship drifted into a distinctly different regime, with much warmer, saltier water in the upper 150 m. We suspect that the eddylike feature seen in the SAR image on day 188 was part of this same upper ocean structure that had remained relatively stationary as wind blew the ice pack over it.

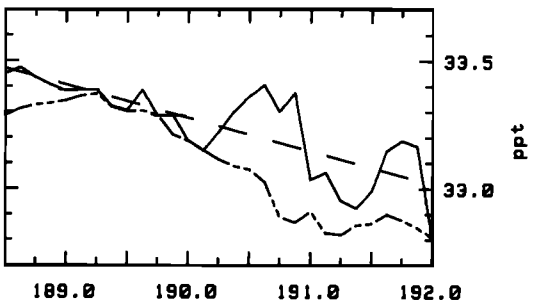

Fig. 4. Average salinity in the water column from 2- to 25-m depth (solid line) and mixed-layer salinity (dashed line). A first-order, least squares fit to the average salinity in the upper 25 m is shown by the broken line.

It is clear from Figure 3 that temperature and salinity structure of the upper ocean beneath the ice floe changed dramatically over the $3\frac{1}{2}$ of the drift. These differences result either from advective changes (e.g., ice drifting across a stationary frontal feature or advection of different water masses by ocean currents) or from time integrals of surface fluxes, distributed in some way by turbulence in the upper ocean. In a drift experiment, separating advective from local changes with any precision is at best difficult and perhaps impossible in the extreme gradients of the MIZ; nevertheless, there are some conservation principles that can be applied to show how far the upper ocean/ice system departed from an ideal, horizontally homogeneous system. First consider upper ocean salinity. At this time of year, water near the ice-ocean interface should freshen as ice melts, unless wind mixing entrains saltier water from below. Wind mixing extends only as far as the turbulence, so in the absence of advection, the total salinity averaged to the maximum entrainment depth should decrease in direct proportion to melting (ignoring precipitation or evaporation). Figure 4 shows the general features described above: during the initial phases of the storm, mixed-layer (defined below) salinity increases by entrainment, against a general decrease in salinity of the upper 25 m, the lower limit of turbulent mixing. If the observed freshening of the upper 25 m were due solely to influx of meltwater at the surface, the slope of the least squares fitted line in Figure 4 would be proportional to the average melt rate, equivalent to about 12 cm d^{-1}. This is several times the melt rate observed before passage of the temperature front; thus local melting could not

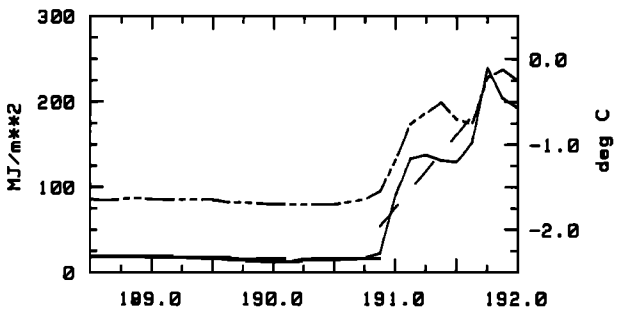

Fig. 5. Heat content for the water column from 2 to 25 m (solid line, scale to left) and mixed-layer temperature (dashed line). Broken line segments indicate first-order, least squares fits to the heat content before and after crossing the temperature front.

account for the observed decrease in salinity between day 188 and day 190, and we infer that a substantial horizontal gradient existed beneath the ice cover south of the *Polar Queen* prior to the storm. After passing the front late on day 190, melt rate increased substantially, and the local melting is more or less consistent with the decrease in upper ocean salinity.

Similar arguments regarding horizontal homogeneity apply to the temperature of the upper ocean. In a horizontally uniform ocean, heating of the water column integrated to the maximum depth of turbulent mixing would be proportional to the incoming radiative energy flux less heat given up to the ice for melting. Figure 5 shows heat content (defined as heat extraction required to lower the water column to its freezing point) in the upper 25 m. Mixed-layer temperature, also shown, follows heat content closely. If turbulence mixes warmer water from below into contact with the ice, heat flux to the ice may exceed incoming radiation, and the layer will cool. This appears to happen during the first part of the drift; however, the entire upper ocean warms during the frontal crossing. Separate least squares line segments fit to the heat content data prior to and following 1800 UT on day 190 have slopes of -1.15 and 172 MJ m^{-2} d^{-1}, respectively. For a horizontally homogeneous process, the first slope corresponds to an energy flux out of the water column of about 13 W m^{-2}, while the second implies energy input of about 2 kW m^{-2}. The quantity of heat contained in the water south of the front was much too large to be explained by local heating. Measurements of ice concentration and incident shortwave radiation on day 191 (Figure 6) indicate that solar input to the ice-ocean system averaged 110 W m^{-2}, of which only 60 W m^{-2} was absorbed in the water A small additional amount (approximately 2–3 W m^{-2}) was added by turbulent transfer from the atmosphere (P. Guest, personal communication, 1986). Although this energy is sufficient to explain about 25% of the melting observed south of the front, it is far too little to account for the increased heat content of the upper 25 m, much less the entire upper ocean. From this we infer that the original ice edge coincided closely with a true water-mass boundary.

4. Boundary Layer Structure

In this section we examine the turbulent structure of the boundary layer and changes in the vertical distribution of density. Our aim is to present the measurements and to point out how they differ from what might be expected if the system were "well behaved" in the sense that horizontal gradients could be ignored. Even with horizontal homogeneity, a rotating boundary layer with rapidly changing surface stress and buoyancy flux, and with a relatively shallow pycnocline, is difficult to describe without resort to quantitative calculations.

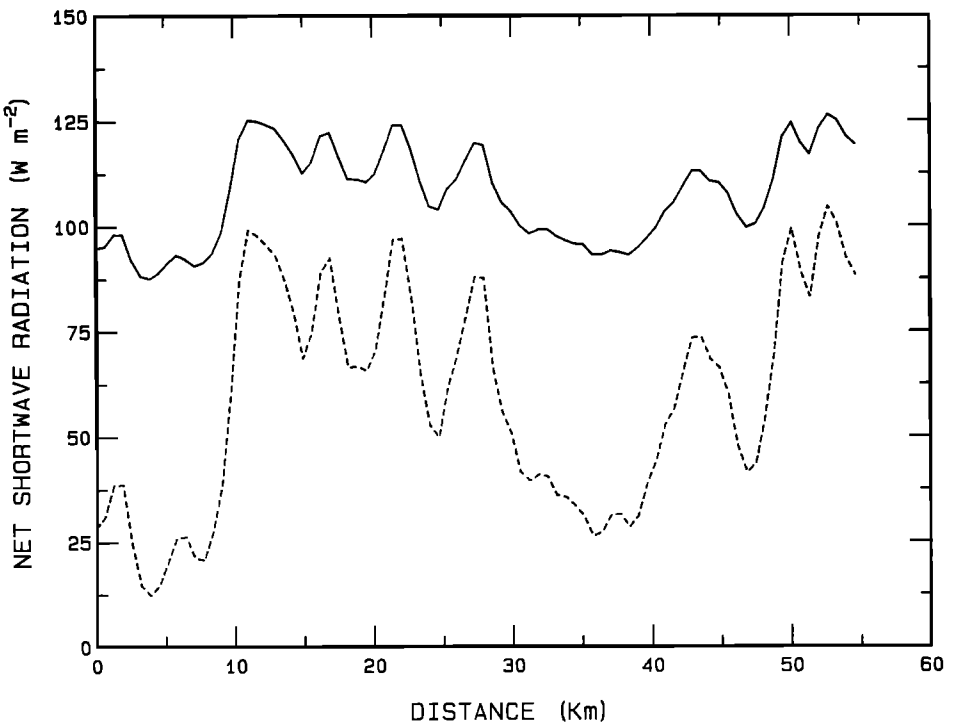

Fig. 6. Net shortwave radiation on day 191 as a function of distance between the *Polar Queen* and the ice edge. Dashed line shows solar input to the upper ocean; solid line is total input to the ice-ocean system.

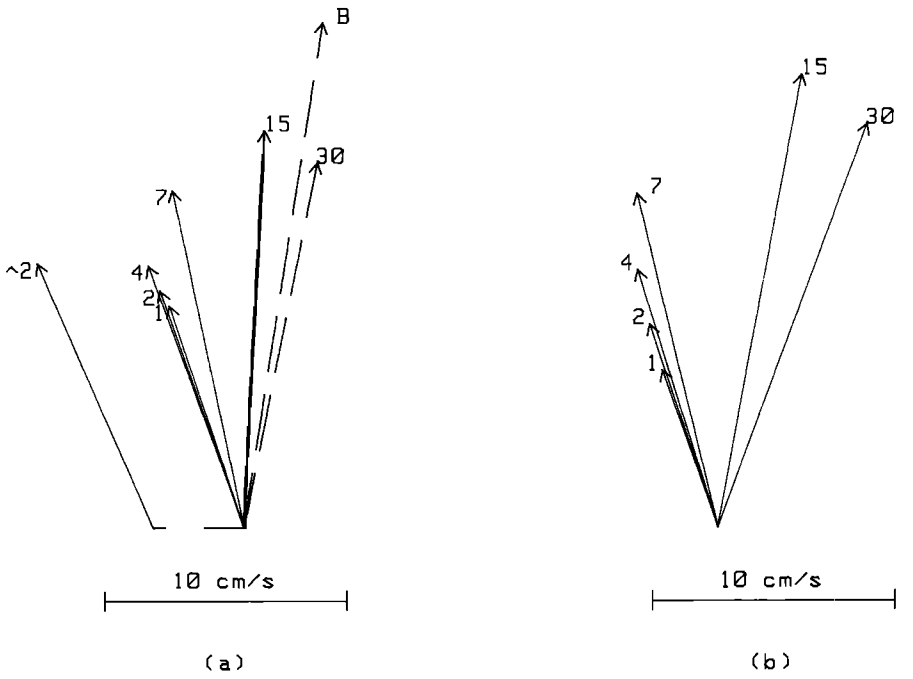

Fig. 7. Plan view of mean current relative to the drifting ice at several levels in the boundary layer. Numbers at vector tips indicate depth (in meters) from the ice underside. North is up. (*a*) Measured mean current for the period 1200 UT, day 188, to 0000 UT, day 192. The separate vector labeled ^2 is from a cluster mounted at 2-m depth approximately 100 m away from the main turbulence mast. Velocity vector labeled B is the negative of the average ice velocity, i.e., the apparent bottom velocity. (*b*) Average modeled velocity with $z_0 = 0.1$ m, transformed into the drifting reference frame.

With this in mind, we use results from a time-dependent, horizontally homogeneous PBL model described in a companion paper [*McPhee*, this issue] to provide some context for interpreting the measurements.

The model includes mass of the ice as a dynamic boundary condition but assumes that the ice drifts freely with no internal stress gradients. Wind stress is obtained from the observed wind, using a drag coefficient ($c_{10} = 0.0023$) calculated from profile measurements made over the ice floe, corrected for stability effects (P. Guest, personal communication, 1986). The ocean below the base of the model domain (50 m) is assumed motionless. Surface buoyancy flux is estimated from the sum of daily average surface and bottom ablation rates. For the storm calculations, the model was initialized to the temperature and salinity structure and surface motion observed at 1200 UT on day 188, and allowed to evolve in response to the observed wind and ice melt.

Measured average values of horizontal velocity and the horizontal component of turbulent stress from each turbulence cluster for the entire period are shown in plan view in Figure 7*a*. Averages were calculated from each 15-min realization of the flow in the 84-hour period. Data are presented in a frame of reference drifting with the ice. One cluster was mounted 2 m below the ice, about 100 m away from the main deployment mast, as shown by the offset vector. The vector labeled B is the apparent velocity of the ocean floor in the drifting reference frame, i.e., the negative of the average ship drift velocity. The dashed vector labeled 30 is the average relative velocity from the filtered APS casts in the period (signal processing for removing tides and inertial currents is described by *Morison et al.* [this issue]). The difference between ice velocity and 30-m current is approximately the surface geostrophic current, about 6 cm s^{-1} to the south, which is consistent with the dynamic topography of the region.

The rightward turning of the mean velocity vectors with increasing depth, which results from the earth's rotation [*Ekman*, 1905], is commonly observed in underice boundary layers [e.g., *Hunkins*, 1966; *McPhee and Smith*, 1976]. The tendency is demonstrated by velocity structure calculated with the horizontally homogeneous model as shown in Figure 7*b*. Vectors at depths corresponding to the measurement levels were generated by averaging model profiles sampled every 3 hours and transformed into a coordinate system moving with the model surface (ice) velocity. The surface roughness, z_0, used in the model is 0.1 m, which is close to the values reported for the AIDJEX camps in the central Arctic by *McPhee* [1979] and slightly larger than found in the Bering Sea MIZ by *Pease et al.* [1983]. Averaged over the whole storm, the observed velocity structure is remarkably similar to the model, implying that nearly all of the current shear in the boundary layer results directly from wind-driven turbulent stress.

The horizontal component of turbulent stress is shown in Figure 8*a*, also in a reference frame relative to the ice, so that the stress vector represents the relative traction from the fluid layer immediately below. Note that stress at each level is to the right of the mean velocity and rotates clockwise with increasing depth, leading the velocity vector: a graphic illustration of the Coriolis effect. There is some question whether the stress at 1 m is representative, because the distance from the underside is comparable to the diameter of the hole through which the frames were deployed. (The effect of the hole may be less significant than it first appears because the horizontal scale of the "energy-containing" eddies is larger than their vertical extent.) The relatively large value of stress at 15 m and

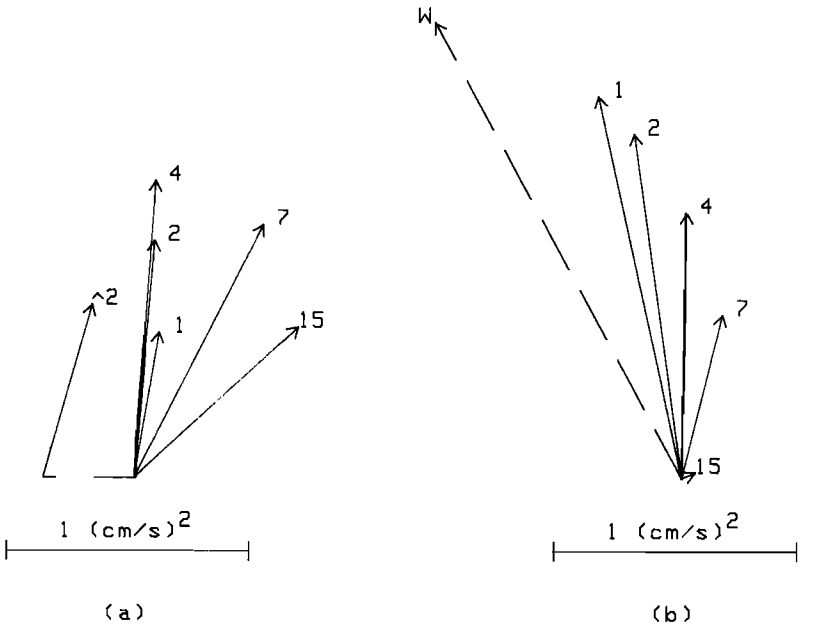

Fig. 8. Plan view of horizontal component of turbulent stress. (*a*) Average of all 15-min realizations of the measured turbulent stress between 1200 UT, day 188, and 0000 UT, day 192. (*b*) Averaged modeled stress for the same period. Vector labeled W is the negative of the average wind stress used to drive the model.

the increase in stress from 1 to 4 m are not present in stress calculated by the numerical model, shown in Figure 8*b*. This and other simple models of turbulent flow over a uniformly rough surface show monotonic decrease of stress away from the interface.

We think the discrepancy between modeled and measured stress results from the nonuniform nature of roughness elements on the ice underside. In this regard, it is useful to consider the differences in scaling between the atmospheric boundary layer above the ice and the underlying oceanic boundary layer. To the atmosphere, sea ice presents a relatively uniform surface with roughness elements 2 orders of mangitude smaller than the boundary layer extent, which is roughly 30 times the oceanic PBL depth. A pressure ridge keel, whose vertical extent is several times that of its sail, is thus 150–200 times as significant in term of its size relative to the boundary layer. The turbulence frames were deployed under relatively smooth ice. Close to the interface, the turbulence is generated from roughness elements within a limited horizontal fetch, but at increasing depths the eddies are larger and presumably reflect more of the true roughness scale. These results suggest that total stress on the ice underside is significantly underestimated by measurements made within 1–2 m of comparatively smooth ice, which reconciles some of the widely varying estimates of underice roughness: an extreme example comes from AIDJEX station Caribou, for which *Langleben* [1980] estimated the underice roughness to be 1.9 mm based on Reynolds stress measurements at 1 m, while *McPhee* [1979] estimated z_0 to be 13.1 cm for the same station, based on wind stress and 2-m mean current.

Stress measurements made deeper than 2 or 3 m below the ice are likely to be more representative of the total stress but should be adjusted to account for expected decrease with depth. The measured and modeled velocity and stress at 4 m, for example, are quite close but smaller than the inferred interfacial stress by about a third. The increased stress levels measured at 7 and 15 m are puzzling but may indicate that the nonuniform undersurface is capable of pushing turbulence deeper than it would otherwise penetrate.

Mean density profiles were calculated for 6-hour periods from APS temperature and salinity profiles (Figure 9*a*). For turbulent mixing, the dynamically important aspect of density is the buoyancy frequency, N, defined by

$$N^2 = -\frac{g}{\rho_0}\frac{\partial \rho}{\partial z}$$

where g is the acceleration of gravity. For purposes of comparison, we define the mixed-layer depth as the first level at which the buoyancy frequency exceeds 4 cph (Figure 9*b*). Toward the end of the period when ice melt is rapid, stratification extends almost to the surface, a situation analogous to the radiatively cooled, nocturnal atmospheric boundary layer. Although a combination of melting and lowered stress will reduce mixed-layer depth, the rapid decrease starting at about noon on day 189 presages the melting associated with the frontal passage and cannot be explained by surface processes.

Figure 9*c* shows numerical model calculations of density structure as buoyancy frequency profiles. The modeled mixed layer deepens rapidly in the first day by mechanical mixing, but since there is no significant increase in melting before day 191, the model does not simulate the mixed-layer shoaling observed from day 190 to 191. After passing over the temperature front, melting increases, so that enhanced buoyancy flux combined with slackening wind stress allow the modeled mixed layer to shoal; however, the stratification is not as pronounced as observed. A plausible explanation is that the ice to the south, which encountered the warm water during a time of more intense turbulence, melted faster, thus stratifying the boundary layer more.

Measurements from a buoy recovered near the ice edge about 56 km south of the *Polar Queen* late on day 189 showed

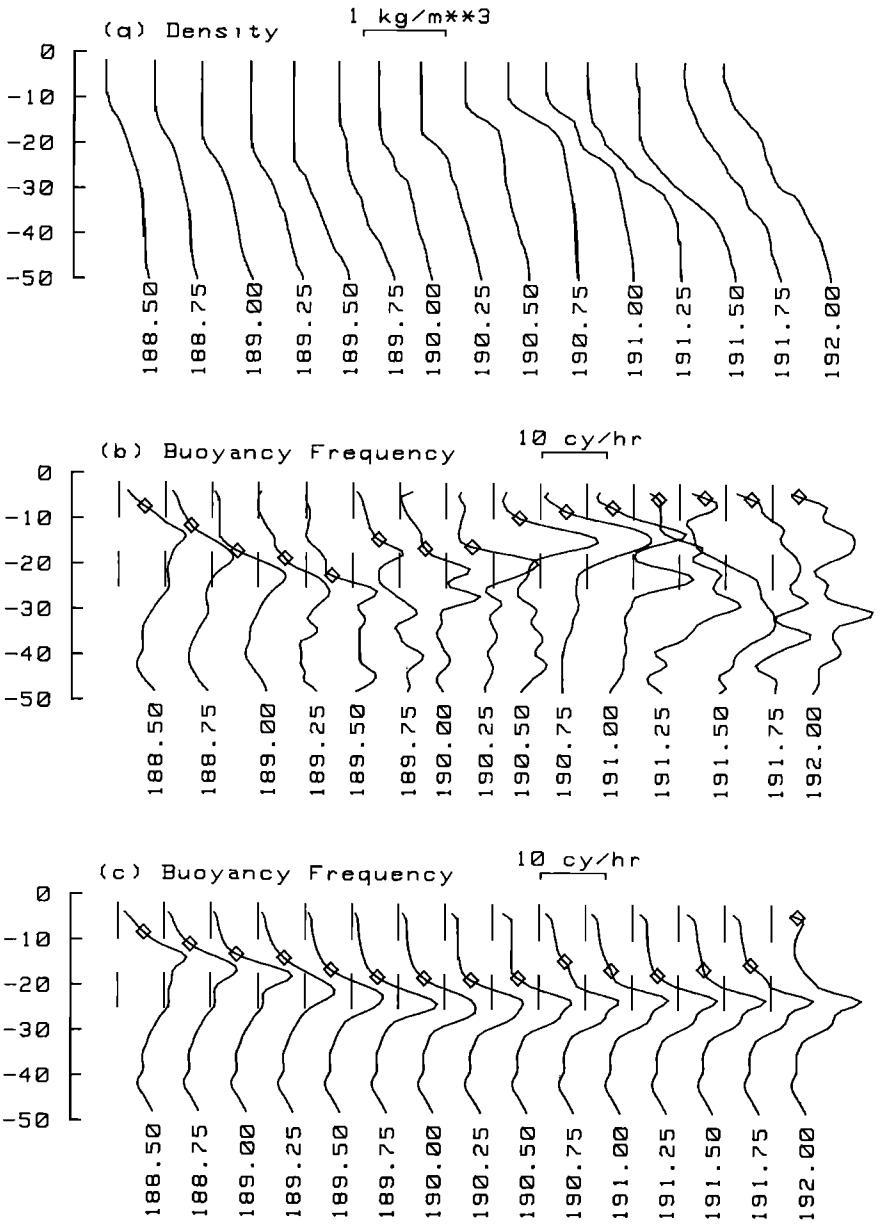

Fig. 9. (*a*) Observed density (sigma zero) profiles, averaged in 6-hour segments. (*b*) Buoyancy (Brunt-Vaisala) frequency corresponding to density profiles of Figure 9*a*, calculated by center differencing, and smoothing with a three-point running mean. Diamonds mark the uppermost level at which the buoyancy frequency exceeds 4 cph ($N = 0.007\ s^{-1}$). (*c*) Buoyancy frequency calculated by the numerical model forced by observed wind stress and ice melt, initialized to temperature and salinity structure at 1200 UT on day 188.

bottom melt in excess of 50 cm in the last 24 hours of its deployment [*Josberger*, 1984]. Buoyancy flux from such extreme melt rates causes a significant increase in surface speed relative to the wind [*McPhee*, 1981; *Mellor et al.*, 1986]. As a rough estimate of the effect, two runs of the numerical model were made. Each was initialized to conditions at 0000 UT on day 189 and run for 24 hours, forced by winds observed near the *Polar Queen*. For the first run, buoyancy flux was determined from the total melt rate as before, while in the second, melt rate was constant at 50 cm d^{-1}. Predicted total displacement (neglecting geostrophic current) for the first run was 20.9 km, compared with 25.4 km for the second (continuous, rapid melting). Bearing of the second trajectory was about 6° right of the first. This phenomenon may account for much of the divergence observed seaward of the *Polar Queen*, but it is also clear that a number of other factors might influence differential drift.

5. Heat and Mass Transfer

As sea ice melts, it introduces fresh or brackish water at the top of the water column, which is buoyant relative to deeper water and therefore affects the dynamics of the boundary layer. How rapidly ice melts by contact with above-freezing water depends on a complex interaction involving heat transport, mass (salinity) transport, momentum flux, and themodynamics of melting at the interface. Our measurements suggest that the physics of heat and mass transport at the interface are strongly affected by molecular exchange in a thin layer immediately adjacent to the interface, and we use our data to derive a relatively simple parameterization of heat and salinity

flux in terms of interfacial stress, and temperature and salinity of the mixed layer.

Sea ice, at least in its macroscopic behavior, is almost always hydraulically rough, i.e., protrusions on the underside are so large that molecular viscosity plays no role in determining the mean velocity profile. For ice, the roughness Reynolds number, $Re_* = u_* z_0/\nu$, where ν is kinematic molecular viscosity, typically ranges from 10^3 to 10^4. Laboratory studies show the transition from smooth to rough flow occurring at Reynolds numbers of less than 100, where the length scale in the Reynolds number is average roughness element size, h [e.g., *Hinze*, 1975, p. 636]. The Nikuradse logarithmic profile

$$\frac{U}{u_*} = \frac{1}{k} \ln \frac{z}{h} + 8.3$$

implies that $h = 30 z_0$. By laboratory criteria, the undersurface of sea ice therefore remains hydraulically rough down to Reynolds numbers of 10 or so, and the momentum boundary layer is unaffected by the viscous sublayer. We might similarly expect that the thermal and concentration boundary layers are insensitive to moleculr effects. Most studies dealing specifically with sea ice have assumed as much, although *Mellor et al.* [1986] argued that surface roughnesses for temperature and salinity would be much smaller than for momentum.

On the other hand, laboratory studies of heat transport and species concentration transport over rough surfaces have shown the importance of molecular effects even at relatively high roughness Reynolds number and have prompted simple models based on conceptually dividing the boundary layer over a rough surface into (1) a thin molecular sublayer in which viscous effects dominate, (2) a transition region influenced by both turbulence and viscous forces, and (3) a fully turbulent region where viscous transport is negligible. The transition sublayer is thought to be about as thick as the dominant scale of the roughness elements, while the molecular sublayer is much smaller. Two models that exemplify the approach are those of *Owen and Thomson* [1963] and *Yaglom and Kader* [1974].

It turns out that neglecting molecular effects for the scalar profiles leads to predicted melt rates that are much larger than we observed. To illustrate this and to show how viscous effects may modify the system, we consider four simple models for heat and salt transfer between the ice and some level in the water column near the interface. For a general framework in which to compare the models, we simplify the surface layer equations by assuming (a) steady state, (b) horizontal homogeneity, and (c) conduction and radiative heating in the ice negligible compared with heat flux from the ocean. The steady, horizontally homogeneous equations for turbulent heat and salinity flux then reduce to

$$\langle w'T' \rangle_0 = wQ_L = -K_h \frac{\partial T}{\partial z} \tag{1}$$

$$\langle w'S' \rangle_0 = w(S_w - S_i) = -K_S \frac{\partial S}{\partial z} \tag{2}$$

where K_h and K_s are diffusivities for heat and salinity, respectively, which include both turbulent and molecular effects; Q_L is the effective latent heat of fusion of sea ice (dependent on ice brine volume) divided by specific heat of seawater; w is the vertical velocity at the top of the boundary layer, related to ice melt rate, d:

$$w = \frac{\rho_i}{\rho_0} d$$

S_W is salinity at the interface. (The subscript w signifies "wall," meaning the immediate interface, as distinguished from properties evaluated at z_0, which may be quite different.) S_i and ρ_i are ice salinity and density near the interface, and ρ_0 is seawater density. (See *Mellor et al.* [1986] for derivation of the boundary flux conditions.)

Equations (1) and (2) may be nondimensionalized and integrated from the interface to an arbitrary level in the turbulent boundary layer to obtain

$$\frac{T(z) - T_w}{wQ_L/u_*} = \Phi_T = \int_z^{z_w} \frac{u_* \, dz'}{K_h}$$

$$\frac{S(z) - S_w}{w(S_w - S_i)/u_*} = \Phi_S = \int_z^{z_w} \frac{u_* \, dz'}{K_s}$$

where Φ_T and Φ_S are nondimensional changes in temperature and salinity from the interface to the level z. The upper limit of integration will vary with the choice of model. At the wall, fluid is at its freezing temperature, related to S_w by the freezing line approximation, $T_w = -mS_w$, where $m = 0.054$, obtained by fitting a straight line to the UNESCO formula [*Gill*, 1982].

If u_*, $T(z)$, and $S(z)$ are known, we have a quadratic equation for S_w and a convenient formula for w in terms of the nondimensional temperature and salinity functions:

$$mS_w^2 + [T(z) + c_2 - mS_i]S_w - [T(z)S_i + c_2 S(z)] = 0 \tag{3}$$

$$c_2 = \Phi_T Q_L / \Phi_S$$

$$w = \frac{u_* [S(z) - S_w]}{\Phi_S (S_w - S_i)} \tag{4}$$

The simplest approach to specifying the nondimensional functions is to assume that flow is fully turbulent, that Reynolds' analogy holds exactly (i.e., $K_h = K_s = K$, the kinematic eddy viscosity), and that buoyancy effects within the logarithmic layer are negligible. Then

$$\Phi_{T,S}^{T1} = \frac{1}{k} \ln \frac{|z|}{z_0} \tag{5}$$

We refer to this as the first turbulent (T1) model. It is essentially the boundary condition used by *Josberger* [1983] and *Ikeda* [1986]. *Mellor et al.* [1986] let the turbulent, logarithmic profiles for temperature and salinity extend to within a much smaller distance from the interface: $z_{0T} = ku_*/\alpha_T$ and $z_{0S} = ku_*/\alpha_s$, where α_T and α_s are molecular heat and salt diffusivities. Thus the second "turbulent" model (T2) is

$$\Phi_{T,S}^{T2} = \frac{1}{k} \ln \frac{|z|}{z_0} + \frac{1}{k} \ln \frac{z_0 k u_*}{\alpha_{T,S}} \tag{6}$$

Owen and Thomson [1963] assumed that the transition sublayer (including the relatively small viscous sublayer) was as thick as the mean roughness element height, h, and that heat flux was proportional to the temperature change across the sublayer times the friction velocity. In the turbulent boundary layer beyond the sublayer, they let the nondimensional temperature profile follow nondimensional velocity (Reynolds' analogy) and used standard dimensional analysis arguments

from heat transfer engineering to describe heat flux across the transition sublayer in terms of a Stanton number, B:

$$\langle w'T' \rangle_0 = Bu_*(T_h - T_w)$$

$$B = \frac{1}{\beta}\left(\frac{u_* h}{\nu}\right)^{-p}\left(\frac{\nu}{\alpha}\right)^{-r}$$

Combining the sublayer and turbulent contributions, the "OT" model is

$$\Phi_{T,S}^{\mathrm{OT}} = \frac{U}{u_*} + \frac{1}{B} = \frac{1}{k}\ln\frac{|z|}{z_0} + \beta\left(\frac{u_* h}{\nu}\right)^{p}\left(\frac{\nu}{\alpha_{T,S}}\right)^{r} \quad (7)$$

If flow is entirely laminar within the sublayer, the Blasius solution provides explicit values for the exponents: $p = 1/2$, $r = 2/3$ [see, e.g., *Incropera and DeWitt*, 1985, chap. 7], but since turbulence affects the transition region in the gaps between roughness elements, *Owen and Thomson* [1963] treated the exponents as empirical constants. By analyzing mainly wind tunnel and roughened-pipe data, they determined that $\beta = 0.52$, $p = 0.45$, and $r = 0.8$ but stressed that β may depend on the particular flow geometry.

Yaglom and Kader [1974] made more explicit use of the viscous sublayer/transition sublayer concept, derived a thickness for the viscous sublayer, and by developing an expression for eddy viscosity beyond the viscous sublayer, integrated the flux equation to the mean roughness height. Their result predicts specific values for the exponents in the Reynolds number and Prandtl number dependencies but requires empirical evaluation of three constants (in addition to the turbulent Prandtl number, assumed to be 0.85), which they obtained using a data base from sources similar to that of *Owen and Thomson* [1963] but expanded substantially. The resulting "YK" expression for nondimensional change in a scalar contaminant is

$$\Phi_{T,S}^{\mathrm{YK}} = \frac{Pr_{\mathrm{Turb}}}{k}\ln\frac{|z|}{z_0} + \left(\frac{u_* h}{\nu}\right)^{1/2}\left\{b_1'\left(\frac{\nu}{\alpha_{T,s}}\right)^{2/3} - b_2'\right\} + C \quad (8)$$

with $b_1' = 0.55$, $b_2' = 0.11$, and $C = 9.5$. Note that for large Prandtl number (ν/α), this expression approaches the viscous sublayer limit, implying that nearly all of the change in the scalar occurs across a thin layer very near the interface.

Equations (5)–(8) are formulas for four different models of Φ_S and Φ_T that may be used in (3) and (4) to estimate melt rate. In each, the first term on the right is the portion of total change in temperature or salinity due to the turbulent boundary layer. The second term is the contribution from the laminar/transition sublayer. To test the different treatments, we used average values for stress and heat flux measured on day 191 (July 9, 1984) compared with mean values of U, T, and S from the clusters mounted 2 m below the ice. Measurements are summarized in Table 1. In determining average heat flux through the mixed layer, we ignored values for the clusters at 15 and 1 m. The former was obviously in more stratified fluid, probably affected by energetic internal wave motion [*Morison et al.*, this issue] and not necessarily indicative of heat reaching the surface. The cluster at 1 m showed anomalously low readings for turbulent stress as well as heat flux and may have been unduly affected by the immediate presence of the hole through which the mast was suspended. Including the 1-m value in the average lowers the mean by about 13%. The error estimate shown in the table is sample standard deviation for the averages of four clusters. An ice core taken from the instrumented floe showed ice salinities in the lowest 30 cm ranging from 3 to 4 ppt (W. Tucker, personal communication, 1986) from which we estimate $S_i = 4$ ppt and brine volume to be 12%. Reducing the latent heat of pure ice (0.3335 MJ kg^{-1}) by the brine volume and using 3980 J kg^{-1} °K^{-1} as the specific heat of seawater, the bottom ice melt corresponding to the average turbulent heat flux is 7.3 cm d^{-1}. Q_L is 74 °K.

TABLE 1. Average Properties for Each Cluster Using All Available Data from Day 191, Average Mixed-Layer Properties, and Average Properties at 2 m

Depth (From Ice), m	Speed, cm s^{-1}	Temperature, °C	Salinity, ppt	q, cm s^{-1}	Heat Flux, W m^{-2}
1	6.64	−0.40	32.84	1.97	75.1
2	8.16	−0.39	32.84	2.37	148.8
2 (remote)	10.64	−0.34	32.84	1.67	142.3
4	9.65	−0.36	32.86	2.51	346.0
7	12.41	−0.30	32.88	2.19	272.5
15	10.82	0.16	33.11	2.41	348.8

Average heat flux, 227 ± 86 W m^{-2}; average u_*, 0.011 m s^{-1}; average $q/2$, 0.011 ± 0.002 m s^{-1}; average bottom melt (day 191), 6.2 ± 3.4 cm; 2-m properties: $U_2 = 0.094$ m s^{-1}; $T_2 = -0.37$°C, and $S_2 = 32.84$ ppt.

Actual bottom melt was estimated from the change in ice thickness measured at interior ablation measurement stations as described by *Maykut and Perovich* [1985]. Readings were taken at about 0800 UT each day, so the value here is the weighted average of the change from days 190–191 and days 191–192. The error shown is sample standard deviation from six sites, each at interior locations within about 50 m of the turbulence frame. Note that variation is large in both the heat flux measurements and ice melt measurements; single-point measurements should be interpreted cautiously.

Friction velocity was calculated from wind stress, modified by the Coriolis force in the ice column, estimated to be 2 m thick. In a separate study [*Morison et al.*, this issue], we found that average root-mean-square turbulent velocity, $q = (\langle u'^2 \rangle + \langle v'^2 + \langle w'^2 \rangle)^{1/2}$, over the entire project was about twice u_* inferred from wind stress, and Table 1 shows that the same holds for this segment of the data. Based on the 2-m current and stress from Table 1, the local roughness length is $z_0 = 0.066$ m. Using u_*, T_2, and S_2 from Table 1, with $\nu = 1.8 \times 10^{-6}$ m^2 s^{-1}, $\alpha_T = 1.3 \times 10^{-7}$ m^2 s^{-1}, and $\alpha_s = 7.4 \times 10^{-10}$ m^2 s^{-1}, and assuming $h = 30z_0$, the nondimensional temperature and salinity functions were calculated for each model, with results summarized in Table 2 (part A).

Melt rates predicted by the fully turbulent models, T1 and T2, are unrealistically high. Since buoyancy effects become increasingly important as the melt rate increases [see, e.g., *McPhee*, 1981], a second set of calculations was made with a buoyancy contribution,

$$\Phi_B = \frac{\beta_L |z|}{kL}$$

added to the turbulent part of nondimensional change, where β_L is the coefficient in the log-linear velocity profile, approximately equal to 5 (we are still assuming Reynolds' analogy)

TABLE 2. Summary of Heat/Mass Flux Model Comparison, Showing Nondimensional Temperature and Salinity Differences Across the Boundary Layer, Salinity at the Interface, and Melt Rate

Model	Φ_T	Φ_S	S_w, ppt	Melt Rate, cm d^{-1}
		Part A		
T1	8.53	8.54	32.31	235
T2	27.8	40.7	32.08	71
OT	301	1.83×10^4	21.44	3.8
YK	346	1.09×10^4	24.45	4.0
		Part B		
T1	22.2	22.2	32.31	89
T2	36.0	49.0	32.12	55
OT	301	1.83×10^4	21.44	3.8
YK	346	1.09×10^4	24.45	4.0

Part A, no buoyancy effects; part B, buoyancy effects included in turbulent part of boundary layer.

and L is the Obukhov length:

$$L = \frac{\rho_0 u_*^3}{kg[\gamma_s \langle w'S' \rangle_0 - \gamma_T \langle w'T' \rangle_0]}$$

where γ_S and γ_T are expansion coefficients for salinity and temperature, respectively. Since the Obukhov length depends on melt rate, solution of the buoyancy contribution is iterative, similar to the technique described by *McPhee* [1983*b*]. Results of these calculations are summarized in Table 2 (part B). As expected, buoyancy reduces heat and salinity flux in turbulent models, but predicted melt rates are still far in excess of observed.

In contrast to the turbulent models, both of the viscous sublayer models underestimate melting. Note that most of the change in scalar quantities occurs within the laminar/transition sublayer. Constants determined for these models followed from laboratory conditions in which roughness was uniform and relatively small. As discussed above, turbulence in the underice boundary layer is apparently affected by roughness elements that are large and irregularly spaced, so that it is plausible that the thickness of the transition sublayer is considerably smaller than $h = 30z_0$. This may account for the discrepancy between laboratory experiments and ours. Reducing z_0, for example, from 6.6 to 1.9 cm in the YK model increases the predicted melt rate to 7.2 cm d^{-1}, close to the value inferred from average heat flux.

The Prandtl number (ν/α_T) and Schmidt number (ν/α_S) in this study are 13.8 and 2432, respectively, larger than the values considered in the OT and YK studies. Following the reasoning of *Yaglom and Kader* [1974], we expect the transition sublayer to behave more like the viscous sublayer at higher Prandtl numbers; thus their Prandtl number dependence ($q = 2/3$) seems preferable to the OT value (0.8). By the same token, at high Prandtl number, the small additive constants in the YK expression, b_2' and C, seem superfluous, and we express the change across the sublayer as

$$\Phi_{T,S}^{\text{vis}} = b\left(\frac{u_* z_0}{\nu}\right)^{0.5} \left(\frac{\nu}{\alpha_{T,S}}\right)^{0.67}$$

By our expression for the Reynolds number dependence, we are assuming that h increases with z_0, although this has not been proved and is open to question. Using mean values from Table 1, with the buoyancy correction for turbulent flow to 2 m, we find a melt rate of 7.3 cm d^{-1} with $b = 1.57$.

In the analysis above, we coupled simple expressions for nondimensional change in T and S across the transition sublayer and the turbulent "surface layer" to find the total change from the interface to the 2-m level and showed that with minor adjustment the models that include a laminar sublayer can predict the observed melt rate. In most applications, a parameterization for heat and salinity flux in terms of mixed-layer properties (i.e., temperature and salinity at the far extent of the turbulent boundary layer) is preferable to one where temperature and salinity are tied to a particular level. We now generalize the procedure to couple a sublayer treatment with an expression for nondimensional scalar change across the turbulent PBL that includes buoyancy effects.

To estimate the nondimensional change in scalar quantities across the turbulent boundary layer, we use a simplification of the theory developed by *McPhee* [1981, 1983*b*]. We assume that the flux of a scalar quantity decreases linearly from its surface value to zero at the boundary layer depth z_{b1}:

$$z_{b1} = -ku_*\eta_*/f$$

with

$$\eta_* = \left(1 + \frac{\xi_N u_*}{fLR_c}\right)^{-1/2}$$

where η_* is a stability parameter, less than or equal to 1, ξ_N is a dimensionless constant (equal to 0.052) and R_c is the critical flux Richardson number (equal to 0.2). Eddy viscosity is given by

$$K = -kzu_* \qquad -z_0 > z \geq z_{s1}$$

$$K = -kz_{s1}u_* \qquad z_{s1} > z \geq z_{b1}$$

$$z_{s1} = -u_*\eta_*^2\xi_N/f$$

For temperature,

$$\frac{T_{b1} - T_a}{\langle w'T' \rangle_0/u_*} = -\frac{1}{k}\int_{z_{s1}}^{-z_0}\left(\frac{1}{z} - \frac{1}{z_{b1}}\right)dz - \frac{1}{kz_{s1}}\int_{z_{b1}}^{z_{s1}}\left(1 - \frac{z}{z_{b1}}\right)dz \qquad (9)$$

The integral of (9) is approximately

$$\Phi_{\text{turb}} = \frac{1}{k}\ln\frac{u_*\xi_N\eta_*^2}{fz_0} + \frac{1}{2\xi_N\eta_*} - \frac{1}{k} \qquad (10)$$

The total nondimensional change is

$$\Phi_{T,S} = \Phi_{\text{turb}} + 1.57\left(\frac{u_* z_0}{\nu}\right)^{0.5}\left(\frac{\nu}{\alpha_{T,S}}\right)^{0.67} \qquad (11)$$

For particular values of u_*, T_{b1}, and S_{b1}, this expression is evaluated first assuming neutral conditions ($\eta_* = 1$), then combined with (3) and (4) to estimate w, which may be used for a refined estimate of Φ_{turb}, and the process repeated until some specified convergence tolerance is met. In practice, the buoyancy effect is minor except at extreme melt rates (because of the large contribution from the laminar sublayer), so that the first estimate is often sufficient.

In Figure 10, measured turbulent heat flux is compared with

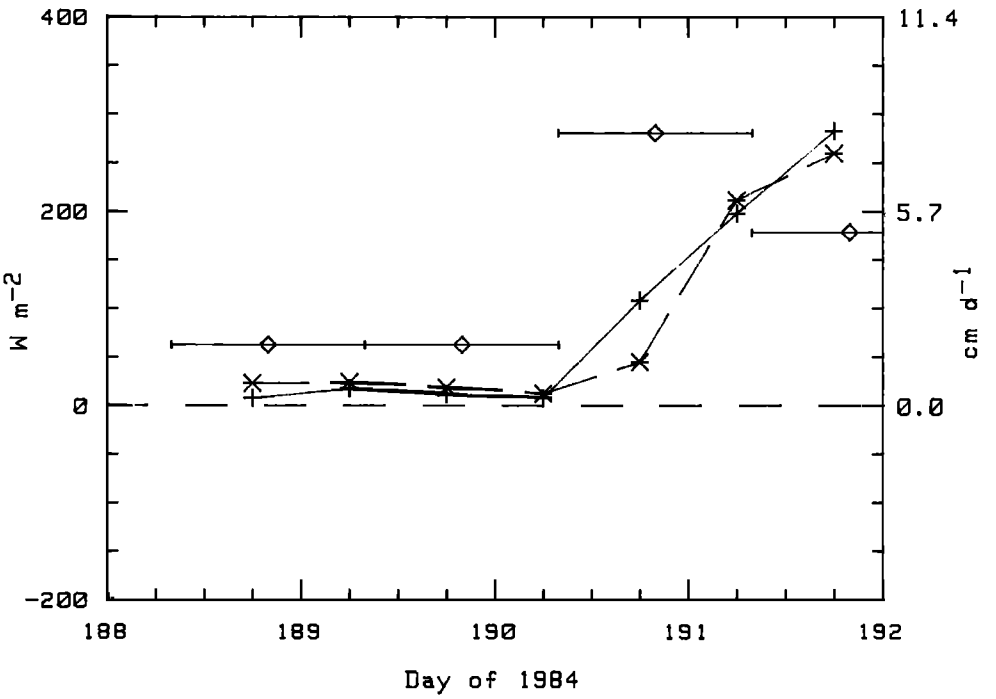

Fig. 10. The solid curve with plus signs is the average vertical component of turbulent heat flux (W m^{-2}) measured with clusters at 2, 4, and 7 m and 2 m remote. The dashed curve with crosses is heat flux inferred from mean temperature, salinity, and turbulent intensity at 4 m, obtained with the model described in the text. The bars with diamonds are daily average values of bottom ablation rate from interior sites, near the turbulence frame.

bottom ablation observed at interior sites and with results predicted by the parameterization developed above. Vertical heat flux was calculated by averaging the 15-min accumulations of $\langle w'T' \rangle$ from clusters at 2 m (both mainframe and remote), 4 m, and 7 m below the ice in 12-hour blocks. The average heat flux in the last day (day 191) was used to set the constant in the transition sublayer Stanton number and is seen to agree reasonably well with heat flux inferred from bottom melt (see also Table 1).

The dashed curve in Figure 10 demonstrates a test of the model, which comprises (10), (11), (3), and (4). Here we considered mean temperature, salinity, and turbulent kinetic energy from one cluster at 4 m as representative of mixed-layer conditions. Friction velocity was estimated to be $q/2$, calculated from velocity variance at 4 m using the same averaging times as above. For each 12-hour period, u_*, T, and S were used to calculate heat flux and resulting melt rate. Except for the last half of day 190, the simple model predicts the measured heat flux very closely. We stress that the dashed curve was predicted using relatively simple measurements (temperature, salinity, and velocity variance) at one level in the boundary layer. The present model is also used by *Morison et al.* [this issue] to estimate melt rates for the entire project, with good results except for a short period near the end of the project, when internal wave drag appears to have been a major factor in the momentum balance.

6. Conclusions

During $3\frac{1}{2}$ days of southward drift, roughly 60 km of pack ice that initially separated the *Polar Queen* from the ice edge preceded it across a temperature front, marking a water-mass boundary in the Greenland Sea MIZ, and we believe that a large proportion of that ice melted during the storm or shortly after. This is an extremely effective ice decay mechanism, and it is likely that much of the mass loss near the extreme edge of the Greenland Sea ice pack east of the Prime Meridian occurs in episodic drifts of this nature and is thus highly correlated with the wind.

Dynamic interactions between ice and water play an important role in the overall mass balance. When ice encounters warm water, its melting stabilizes the boundary layer and increases surface velocity, so that ice near the margin separates from the interior. Divergence of the ice pack hastens melting by opening the ice-covered ocean to enhanced insolation, by exposing more edge surface to water contact, and by sending ice farther out over warm water. Near the edge, melt rates are extreme when the ice encounters warm water. We found, however, that ice could survive for extended periods in water at least a degree above freezing, even when turbulence levels were high, in contradiction to the results of several recent models. The reason for this appears to be that, unlike ice-ocean momentum flux, heat and mass transfer are strongly affected by a thin sublayer controlled by molecular processes, even if the undersurface is hydraulically rough. We have suggested a simple model that incorporates these concepts.

Results from the MIZEX drift experiment have important implications for numerical modeling of the ice-edge region. It is clear that buoyancy effects associated with preconditioning of the boundary layer (e.g., by previous melting, by wind mixing, by advection of warm water) can have major impact on the dynamics of ice motion and the thermodynamics of mass balance in the MIZ. A simple set of exchange coefficients cannot be expected to yield accurate estimates of melt rate or ice velocity where stratification varies as much in time and space as in the MIZ. To ignore these effects in numerical models of ice-edge processes seems to us naive.

Water-mass boundaries in the Greenland Sea appear to be constrained by bathymetry, and annual variations of ice extent are small relative to the Southern Ocean and other marginal seas in the Arctic. Comparison of measurements with results from horizontally homogeneous modeling shows that the existence of definite water-mass boundaries has a controlling influence on ice-edge position. Our study thus indicates that location of the ice edge in the Greenland Sea is largely determined by the seasonally varying balance between northward and westward advection of near-surface oceanic heat, and southward and eastward wind-driven ice drift.

Acknowledgments. K. Davidson and P. Guest of the Naval Postgraduate School provided the atmospheric drag coefficient and heat flux data. G. Mellor of Princeton University pointed out the relevance of the *Owen and Thomson* [1963] and *Yaglom and Kader* [1974] work and supplied other much appreciated advice. The research was supported by the Office of Naval Research, under contracts N00014-84-C-0111, N00014-78-C-0135, and N00014-84-C-0028. The paper is dedicated to the memory of Arne Hanson, who performed the mass balance field work, and whom we all miss.

References

Ekman, V. W., On the influence of the earth's rotation on ocean currents, *Ark. Mat. Astron. Fys., 2*, 1–52, 1905.

Gill, A. E., *Atmospheric-Ocean Dynamics*, 661 pp., Academic, Orlando, Fla., 1982.

Hall, R. T., MIZ84 *Polar Queen* helicopter photography, *Data Rep. APL-UW 10-84*, Univ. of Washington, Seattle, 1984.

Hinze, J. O., *Turbulence*, 2nd ed. 790 pp., McGraw-Hill, New York, 1975.

Hunkins, K., Ekman drift currents in the Arctic Ocean, *Deep Sea Res., 13*, 607–620, 1966.

Ikeda, M., A mixed layer beneath melting sea ice in the marginal ice zone using a one-dimensional turbulent closure model, *J. Geophys. Res., 91*, 5054–5060, 1986.

Incropera, F. P., and D. P. DeWitt, *Fundamentals of Heat and Mass Transfer*, 2nd ed., 802 pp., John Wiley, New York, 1985.

Johannessen, O. M., Note on some vertical profiles below ice floes in the Gulf of St. Lawrence and near the North Pole, *J. Geophys. Res., 75*, 2857–2861, 1970.

Josberger, E. G., Sea ice melting in the marginal ice zone, *J. Geophys. Res., 88*, 2841–2844, 1983.

Josberger, E. G., Extreme ice edge ablation studies, MIZEX Bulletin 4, *CRREL Spec. Rep. 84-29*, pp. 74–75, U.S. Army Cold Regions Res. and Eng. Lab., Hanover, N. H., 1984.

Josberger, E. G., Bottom ablation and heat transfer coefficients from the 1983 Marginal Ice Zone Experiments, *J. Geophys. Res.*, this issue.

Josberger, E. G., and D. Meldrum, Bottom ablation measurements and heat transfer coefficients from MIZEX-West, February 1983, MIZEX Bulletin 6, *CRREL Spec. Rep. 85-6*, pp. 68–72, U.S. Army Cold Regions Res. and Eng. Lab., Hanover, N. H., 1985.

Langleben, M. P., Water drag coefficient at AIDJEX, station Caribou, in *Sea Ice Processes and Models*, edited by R. S. Pritchard, pp. 464–471, University of Washington Press, Seattle, 1980.

Langleben, M. P., Water drag coefficient of first-year sea ice, *J. Geophys. Res., 87*, 573–578, 1982.

Maykut, G. A., and D. K. Perovich, MIZEX 84 heat and mass balance data, *Data Rep. APL-UW 12-85*, 73 pp., Univ. of Wash., Seattle, 1985.

McPhee, M. G., The effect of the oceanic boundary layer on the mean drift of pack ice: Application of a simple model, *J. Phys. Oceanogr., 9*, 388–400, 1979.

McPhee, M. G., An analytic similarity theory for the planetary boundary layer stabilized surface buoyancy, *Boundary Layer Meteorol., 21*, 325–339, 1981.

McPhee, M. G., Greenland Sea ice/ocean margin, *Eos Trans. AGU, 64*, 82–83, 1983*a*.

McPhee, M. G., Turbulent heat and momentum transfer in the oceanic boundary layer under melting pack ice, *J. Geophys. Res., 88*, 2827–2835, 1983*b*.

McPhee, M. G., Comment on "Sea ice melting in the marginal ice zone," by Edward G. Josberger, *J. Geophys. Res., 89*, 759–760, 1984.

McPhee, M. G., Analysis and prediction of short-term ice drift, in *Proceedings of the Fifth International Offshore Mechanics and Arctic Engineering Symposium*, pp. 385–393, vol. 4, American Society of Mechanical Engineers, New York, 1986*a*.

McPhee, M. G., A velocity/temperature/conductivity measuring system for the underice ocean environment, in *Proccedings of the IEEE Third Working Conference on Current Measurement*, edited by G. F. Appell and W. E. Woodward, pp., 215–220, Institute of Electrical and Electronics Engineers, New York, 1986*b*.

McPhee, M. G., A time-dependent model for turbulent transfer in a stratified oceanic boundary layer, *J. Geophys. Res.*, this issue.

McPhee, M. G., and J. D. Smith, Measurements of the turbulent boundary layer under pack ice, *J. Phys. Oceanogr., 6*, 696–711, 1976.

Mellor, G. M., M. G. McPhee, and M. Steele, Ice-seawater turbulent boundary layer interaction with melting or freezing, *J. Phys. Oceanogr., 16*(11), 1829–1846, 1986.

Morison, J. H., The Arctic Profiling System, Proceedings of a Working Conference on Current Measurement, *Tech. Rep. DEL-SG-3-78*, pp. 311–318, Coll. of Mar. Stud., Univ. of Del., Newark, 1978.

Morison, J. H., Forced internal waves in the Arctic Ocean, Ph.D. thesis, 289 pp., Geophys. Program, Univ. of Washington, Seattle, 1980.

Morison, J. H., and J. D. Smith, Seasonal variations in the upper ocean as observed at T-3, *Geophys. Res. Lett., 8*, 753–756, 1981.

Morison, J. H., M. G. McPhee, and G. A. Maykut, Boundary layer, upper ocean, and ice observations in the Greenland Sea marginal ice zone, *J. Geophys. Res.*, this issue.

Owen, P. R., and W. R. Thomson, Heat transfer across rough surfaces, *J. Fluid Mech., 15*, 321–334, 1963.

Pease, C. H., Eastern Bering Sea processes, *Mon. Weather Rev., 108*, 2016–2023, 1980.

Pease, C. H., S. A. Salo, and J. E. Overland, Drag measurements for first-year sea ice over a shallow sea, *J. Geophys. Res., 88*, 2853–2862, 1983.

Smith, J. D., Turbulent structure of the surface boundary layer in an ice-covered ocean, *Rapp. P. V. Reun. Cons. Int. Explor. Mer, 167*, 53–65, 1974.

Smith, J. D., Measurement of turbulence in ocean boundary layers, Proceedings of a Working Conference on Current Measurement, *Tech. Rep. DEL-SG-3-78*, pp. 95–128, Coll. of Mar. Stud., Univ. of Del., Newark, 1978.

Untersteiner, N., and F. I. Badgley, The roughness parameters of sea ice, *J. Geophys. Res., 70*, 4573–4577, 1965.

Yaglom, A. M., and B. A. Kader, Heat and mass transfer between a rough wall and turbulent fluid flow at high Reynolds and Peclet numbers, *J. Fluid Mech., 62*, 601–623, 1974.

G. A. Maykut, Department of Atmospheric Sciences, University of Washington, Seattle, WA 98195.

M. G. McPhee, McPhee Research Company, 371 Rolling Hills Drive, Yakima, WA 98908.

J. H. Morison, Polar Science Center, University of Washington, Seattle, WA 98195.

(Received July 7, 1986;
accepted December 3, 1986.)